Eur. Phys. J. B **13**, 755–763 (2000)

THE EUROPEAN PHYSICAL JOURNAL B

EDP Sciences
© Società Italiana di Fisica
Springer-Verlag 2000

Experimental feasibility of phaseless inverse scattering methods for specular reflectivity

A. van der Lee[a]

Laboratoire des Matériaux et Procédés Membranaires[b], 8 rue de l'École Normale, 34296 Montpellier Cedex 5, France

Received 19 May 1999

Abstract. The possibilities for calculating the X-ray or neutron scattering potential across a thin film from experimental specular reflectivity amplitude information alone and using full dynamical theory, *i.e.*, phaseless inverse scattering, are investigated and compared with traditional fitting methods. The feasibility of the method is demonstrated by one trivial and two non-trivial experimental examples. The usefulness, but also the limitations are outlined by the experiments and by numerical examples. The data reduction is treated in some detail and, in particular, a new method is proposed for deconvolving the experimental data from the instrumental smearing function.

PACS. 61.10.Kw X-ray reflectometry (surfaces, interfaces, films) – 68.35.Ct Interface structure and roughness – 68.55.Jk Structure and morphology; thickness

1 Introduction

The determination by specular neutron or X-ray reflectivity of the scattering potential (SP) $V(z)$ perpendicular to an interface has become a routine tool in surface and thin film science. Reflectivity data have been traditionally analyzed by trial-and-error and non-linear least squares fitting methods using Parrat's recursive reflectivity calculation method [1] to arrive at the final SP perpendicular to the surface. The dependency of these fitting methods on an *a priori* postulated model finds its origin in the fact that normally only the amplitudes of the reflected waves can be measured and not their phases. This is called the phase problem and has its equivalence in, *e.g.*, crystallography.

A second problem is that the SP is quite difficult to calculate from the complex reflection coefficient even if the phases were known, because of the dynamical nature of the reflectivity scattering process in the vicinity of the critical angle for total reflection. This is called the inverse scattering (IS) problem and does not have an analog in crystallography. In crystallography the Born approximation for scattering can be assumed to be valid so that the scattering density can be calculated by an inverse Fourier Transform from the complex scattering data. Both the phase problem and the IS problem are naturally circumvented if an *a priori* model is assumed that is adjusted by hand and/or by least-squares to get agreement with the experimental data. These fitting methods are, however, quite difficult to employ in the case of non-trivial SP's, and need not give a unique solution. Hence the need arises for a more model-independent determination of the SP by specular reflectivity.

Several model-independent approaches have been proposed during the last years that aim to go beyond the Born approximation for specular reflectivity. They can be classified according to whether they are based on a fitting procedure or on an *ab initio* calculation using inverse scattering theory. Fitting procedures based on the distorted wave born approximation (DWBA) have been proposed by Sanyal *et al.* [2] and those based on an expansion of the SP in a basic set of functions by Pedersen and Hamley [3] and Berk and Majkrzak [4]. They have in common that the resulting SP need not be unique.

On the contrary, inverse scattering methods claim to solve the IS problem and to yield a unique SP at the condition that the phase is known by some means. The first proposals to measure indirectly the phase by performing one or two additional measurements on systems with magnetic reference layers were from de Haan *et al.* [5] and Majkrzak and Berk [5,6]. They have only recently found application [7,8]. Meanwhile, other methods have been proposed using non-magnetic reference layers that can also be employed in the X-ray case by either varying the wavelength across the absorption edge of one of the constituting elements [9,10] or by contrast variation using one or two different reference layers [11–13]. The contrast variation method for non-magnetic reference layers have not yet found applications.

Methods that do not use additional measurements and/or reference layers have been proposed by Klibanov and Sacks [14] and by Clinton [15]. These methods are called phaseless inverse scattering (PIS) methods, since

[a] e-mail: avderlee@crit1.univ-montp2.fr
[b] UMR 5635 du CNRS

they calculate the SP from the experimental data without explicit phase information from elsewhere. Phase information is assumed to be implicitly present in the amplitude information and is extracted by mathematical means. The advantage of PIS methods is, of course, that the system to be studied is not disturbed by the presence of a reference layer and that the data collection can be performed, in general, in any laboratory equipped with a commercial or home-built diffractometer. Another advantage of PIS is that the mathematical data treatment is less laborious than that for two- or three measurement methods. The drawback is that some physical pre-information is required to judge the uniqueness of the result. It should be noted, however, that the methods proposed to determine the phase uniquely quite often give two alternative solutions as well, from which one has to be rejected on physical grounds as well [8,11,13]. A second disadvantage is that not every system is suitable for SP determination by PIS.

Although an experimental determination of the phase of the reflected waves by one of the methods mentioned before is preferable from a theoretical point of view, it is anyhow of interest to see in what circumstances PIS methods could be used to extract meaningful information from a reflectivity experiment. Clinton [15] envisioned PIS methods to play a complementary role to traditional modeling techniques, but to date it has not been shown how this is realized in practice.

The goal of this paper is to show in which experimental circumstances and for which kind of systems PIS might be useful for SP determination by specular reflectivity and to explore the experimental factors that influence the data reduction. In addition a new method is proposed for deconvolving the experimental data from the instrumental smearing function. This deconvolution method could not only be useful for phaseless inverse scattering but also for SP determination by more general inverse scattering methods using reference layers.

2 Data reduction and analysis

The PIS data reduction procedure is outlined in Figure 1 and is contrasted with the fitting methods that are either model-dependent or model-independent. The first step involves the reduction of the raw data $I(k)$, *viz.*, scaling, subtracting noise and eventual diffuse scattering, to get the (convolved) square of the reflection coefficient $r_{\mathrm{CV}}(k)$. The intensity reduction due to geometric effects for angles below the critical angle [16] is simply ignored and all intensity data for angles below the angle at the plateau of total reflection where the intensity is maximum is set to 1.00. All subsequent data are scaled accordingly. No data smoothing is performed.

The second step involves the deconvolution of the experimental data r_{CV}. Deconvolution is not necessary if a fitting approach is used, whether it is model-dependent based on Parrat's recursive method or model-independent using a DWBA-approach or spline-functions, since then the reflectivity data are generated from the model and subsequently convolved with the instrumental profile function IPF. The convolved data are compared with the experimental data, and the starting set of parameters is adjusted by least-squares analysis (Fig. 1b). If, however, an *ab initio* approach is sought using IS methods, deconvolution of the experimental data becomes indispensable if details in the reflectivity are smeared out by the IPF. Since the deconvolution of experimental reflectivity data is not well documented in literature, a new method is here proposed that appears to work well.

The instrumental profile function (IPF), which smears the experimental data, is determined by factors like slit width and height, beam divergence, wavelength spread and the presence of optical elements like monochromators and analyzers. The smearing operation is normally represented by the convolution integral:

$$r_{\mathrm{CV}}(k) = P[r_{\mathrm{DC}}(k)] = \int_{-\infty}^{\infty} r_{\mathrm{DC}}(k-\kappa) IPF(\kappa) \mathrm{d}\kappa. \quad (1)$$

Here P is the convolution operator and $r_{\mathrm{DC}}(k)$ is the non-convolved square of the reflection coefficient: $r_{\mathrm{DC}}(k) = |R(k)|^2$. k (and κ) is the z-component of the incident wave vector: $k = 2\pi \sin\theta/\lambda$ with θ the angle between incident beam and the surface and λ the wavelength. It is noted that the momentum transfer q of the scattering process is equal to $q = 2k$. Appropriate treatments of instrumental profile functions for X-ray [16] and neutron reflectometers [17] can be found in the literature. Most often, a Gaussian smearing function is used.

Although the convolution operator P itself is straightforward to apply, the inverse operator P^{-1} is usually highly ill-conditioned [18]. Deconvolution techniques, which have a large tradition in especially astronomy, are either based on regularisation techniques that try to stabilize the inversion of large matrices, or on iterative techniques that convolve a test solution and compare it with the experimental data, then improve the test solution etc. For specular reflectivity data none of the existing methods appeared to be satisfactory alone. Instead, a combination of a technique based on zeroth-order Tikhonov regularisation [18] (TR) and the original Lucy-Richardson algorithm [19,20] (LR) gave the best results.

First, two solutions r_{TR} and r_{LR} are calculated, based on TR and LR, respectively. The best TR-solution is selected by varying the regularisation parameter until a minimal figure of merit is found. The figure of merit is defined by $\mathrm{FOM} = |\sum_{i=1}^{i=N/2}(r_{\mathrm{CV}}(i) - P[r_{\mathrm{DC}}(i)])^2|$, if N is the number of data. The LR-iteration is stopped when the relative change in the figure of merit is smaller than 10^{-4}. The sum is over the first half of the data points, because it was observed that the LR solution deteriorates at the end of the interval with increasing number of iterations. On the other hand, the TR solution appears to be very good in the second half of the interval, but not very stable for angles close to the critical angle, where the variation of the reflectivity is largest. There the calculated TR-solution $r_{\mathrm{TR}}(i)$ quite often tends to get negative. Therefore, an optimal deconvolved $r_{\mathrm{DC}}(i)$ is selected out

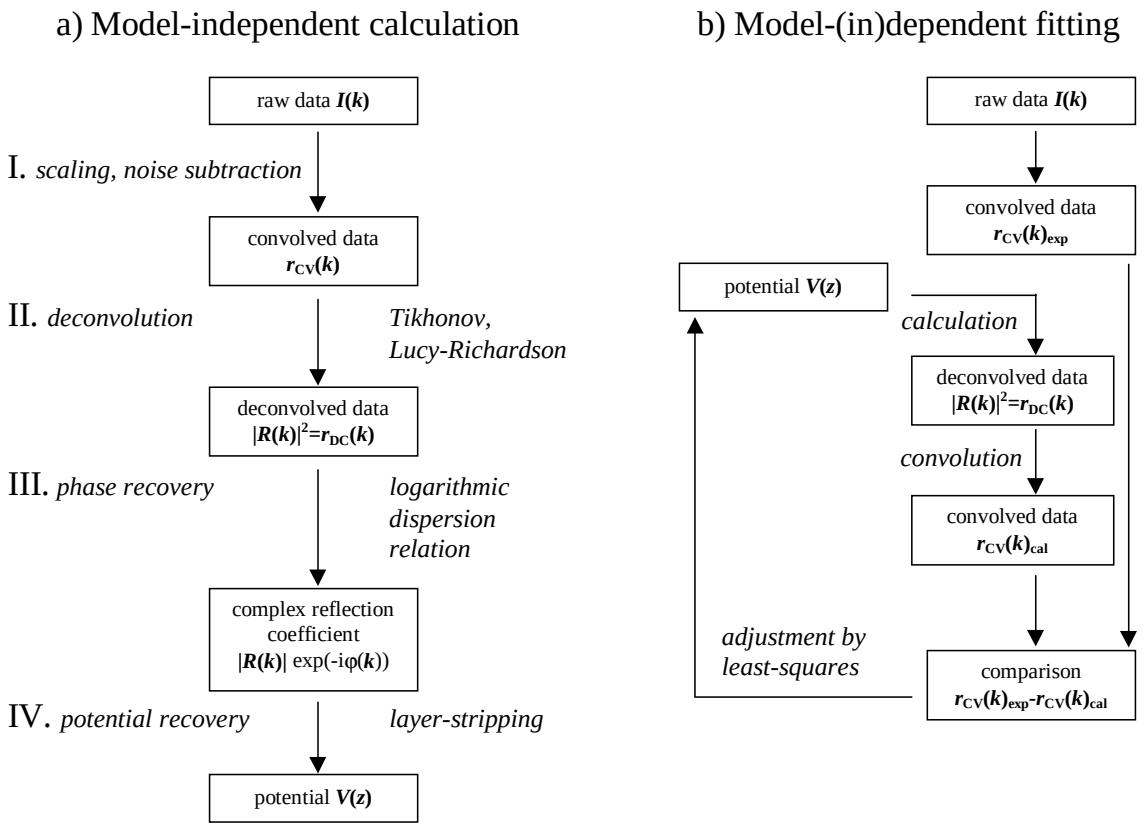

Fig. 1. Flow diagrams showing reflectivity data treatment for (a) PIS and (b) least-squares modeling.

of the TR and LR solutions $r_{\rm TR}(i)$ and $r_{\rm LR}(i)$, based on criteria like positiveness, smoothness and best individual figure of merit $IFOM(i) = (r(i) - P[r(i)])^2$. A solution is rejected when it is negative or when subsequent solutions $r(i)$ and $r(i+1)$ differ by more than a factor 10. In the considered cases, subsequent data values of the theoretical non-convolved reflectivity curves never differed more than a factor 10 using reasonable (experimental) step sizes. These two criteria, the smoothness and positivity criterion were found to apply only to the TR solution. Next, the values of $IFOM_{\rm TR}(i)$ and $IFOM_{\rm LR}(i)$ are compared. If $IFOM_{\rm TR}(i)$ is better, the TR-solution $r_{\rm TR}$ is selected; if $IFOM_{\rm LR}(i)$ is better, the LR-solution $r_{\rm LR}$ is taken as the deconvolved signal $r_{\rm DC}$. Finally, the complete deconvolved solution is scanned to see if there are no single or double TR-solution values within an otherwise continuous range of LR-solutions. This criterion is again based on smoothness, and has to be applied because of the non-uniqueness of the deconvolution operation P^{-1}. $IFOM_{\rm TR}(i)$ might be smaller than $IFOM_{\rm LR}(i)$ because of a second solution which happens to be better than the true solution, but this solution appears not to be smooth with the surrounding solutions. Such false TR-solutions are therefore interchanged by LR-solutions.

This deconvolution algorithm was tested on simulated data for two realistic cases, the first one being a 47 nm tungsten film on a Si substrate capped by a 5 nm layer Si layer with a 2 nm thick oxidized surface layer, the second one being a W/Si/W/SiO_2 multilayer with 13.0, 7.0, 13.5, and 9.0 nm thick individual layers, respectively, on a Si substrate, with 0.7, 0.7, 0.5, 0.5, and 0.5 nm as roughness parameters for the respective interfaces. It is noted that in all calculations and figures in this paper the scattering potential $V(z)$ is used, rather than the scattering length density $\rho(z)$. The relation between $V(z)$ and $\rho(z)$ is simple: $V(z) = 4\pi\rho(z)$. A Gaussian smearing function was used [16]:

$$IPF(\kappa) = \exp(-\kappa^2/2\sigma^2) \qquad (2)$$

with σ equal to the half width at half maximum of the main beam. The algorithm was tested by going through the complete IS calculation (Fig. 1a).

Figure 2a shows the (neutron) reflectivity $r_{\rm CV}$ of the tungsten layer after convolving it with the IPF (upper curve), the original non-convolved reflectivity $r_{\rm TH}$ (middle curve), and the reconstructed deconvolved reflectivity $r_{\rm DC}$ (lower curve). The inset in the right upper corner shows that for large k-values the reconstructed curve is indistinguishable from the original curve. For k-values around the critical edge (left lower corner inset) some deviations are visible. Figure 2b shows the reconstructed (neutron) SP's from these three reflectivity curves, using the PIS method. It is seen that deconvolution is indispensable, since the reconstructed potential $V_{\rm CV}$ from the convolved data $r_{\rm CV}$ is heavily affected by the instrumental smearing. The reconstructed potential $V_{\rm DC}$ from the deconvolved data $r_{\rm DC}$ is quite close to the theoretical reconstructed potential,

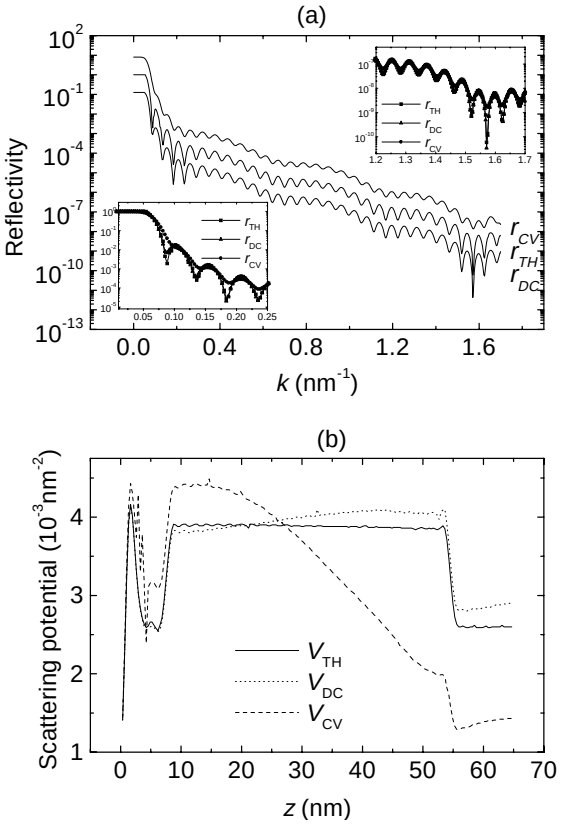

Fig. 2. (a) Calculated neutron reflectivity for a 47 nm thick tungsten layer on a silicon substrate, capped by a 5 nm thick Si layer with a 2 nm oxidized surface layer. Upper curve: convolved data; middle curve: theoretical unconvolved data; lower curve: deconvolved data. The two insets show some parts of the data interval in more detail. (b) Reconstruction of the SP using the data of (a).

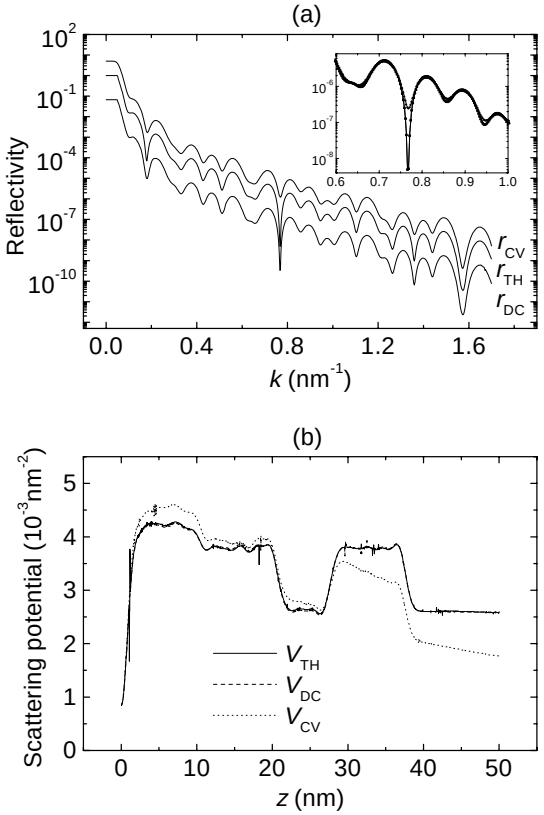

Fig. 3. (a) Calculated neutron reflectivity for a W/Si/W/SiO_2 multilayer on a silicon substrate. Upper curve: convolved data; middle curve: theoretical unconvolved data; lower curve: deconvolved data. The inset show a part of the data interval in more detail. (b) Reconstruction of the SP using the data of (a).

except for a small deviation around the substrate/film interface. This is related to the not so perfect deconvolution around the critical edge. It is noted that the singularities of the thin film perpendicular structure, *viz.*, the jumps in the scattering potential, remain visible even after severe smearing. The thickness of the tungsten film can be determined with precision. This appears to be a generality of PIS methods for quite general SP's: the reflection amplitudes alone (without phases) contain sufficiently enough information to determine the location and amplitude of singularities in the SP [21]. This was strictly speaking only proved for unconvolved signals, but seems to apply as well to the convolved signal.

Figures 3a and 3b show the reflectivity curves and the reconstructed scattering potentials for the multilayer. Here, instrumental smearing is less severe, because of the thinner layers compared to those of the tungsten example. The reconstructed potential using the deconvolved data r_{DC} coincides nearly completely with V_{TH}, also for z-values within the substrate, since deconvolution is now fairly good in the neighborhood of the critical edge. The reconstruction itself, even the theoretical one, V_{TH}, is on the other hand less good than that of the tungsten example, indicating that the maximum value $k_{\max}$ have been taken too small.

The third step in the data analysis (Fig. 1a) concerns the determination of the phase $\arg(R(k))$, either by means of independent data from a second and sometimes from a third measurement, or, in certain cases, mathematically by means of a logarithmic dispersion relation. Here the form proposed by Klibanov and Sacks [14] was used:

$$\arg(R(k)) = -\pi + \frac{1}{2\pi}\int_{-1}^{1} \log\left[\frac{r(k)r(1/\kappa)}{r(k+\kappa)r(k+1/\kappa)}\right]\frac{\mathrm{d}\kappa}{\kappa}\,. \tag{3}$$

The data r are the experimental reflectivity data points r_i (if necessary desmeared) interpolated by cubic B-splines to get a quasi-continuous reflectivity function. This interpolation is necessary because the integrand of the integral in equation (3) requires data at points k_i that have not been measured. The interpolation does not give problems at the condition that the step Δk_i is not too large. This means in practice that in order to correctly describe an interference fringe Δk_i should be taken to be about one tenth of the period of the fringe. It is also advisable to take a small step in the vicinity of the critical edge, since

there the reflectivity changes drastically. The singularity of the integrand of equation (3) at $\kappa = 0$ is dealt with in the way described by Klibanov and Sacks [14]. Data required beyond the experimental cut-off are estimated by the asymptotic form $r(k) \sim (V_0/k^2)^2$, in which the constant V_0 itself is estimated from the last part of the experimental data interval. The exact value of V_0 is not very critical, at the condition that the data have been measured sufficiently far. The integration itself is performed by the extended trapezoidal rule. More sophisticated quadrature algorithms do not improve the accuracy of the final result. Results obtained by using equation (3) will be discussed further in the following section.

Finally, the SP can be calculated using the values of $|R(k)|$ and $\arg(R(k))$. Different methods have been proposed [22–24], all of which are inherently instable for "large potentials" [25]. In this paper Sack's layer-stripping method was used, which is believed to be more stable than the other methods [23]. The instability of this last inversion step can be considered to be the most serious obstacle for the use of IS methods in general, since it implies that SP's of thin films larger than about 20 nm for X-rays or about 100 nm for neutrons, cannot be determined anymore, if silicon is assumed to be the substrate. These numbers depend of course on the exact scattering power of the elements that constitute the film. Some work is being performed, however, to find alternative ways to analyze the inherent instability of inverse scattering [26] based on Lyapunov exponents. This may yield new ways to shift the outset of instability to larger potentials.

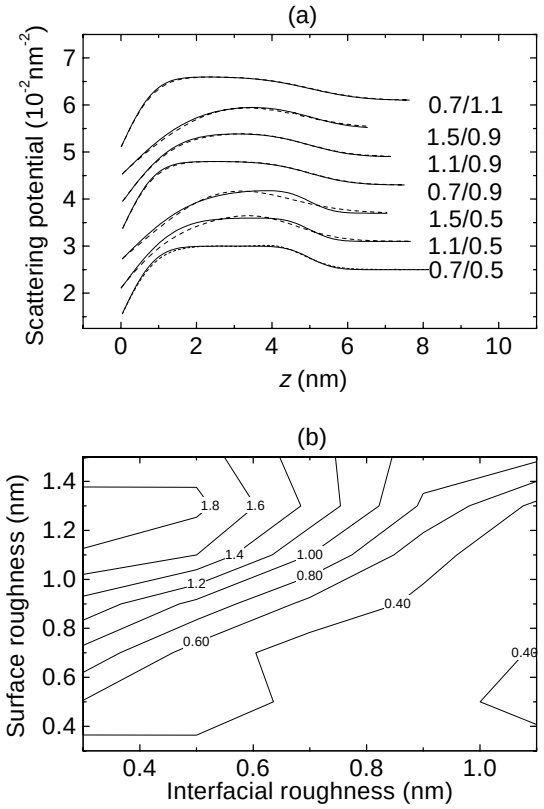

Fig. 4. (a) Reconstructions (dashed curves) of typical X-ray SP's (full curves). The numbers shown are the values for the surface and interfacial roughness, respectively. (b) shows the relative percentual error of the reconstruction as a function of the interfacial roughness (x-axis) and the surface roughness (y-axis).

3 Phaseless inverse scattering

The phase obtained by equation (3) is unique if two conditions are fulfilled. The first one supposes that the potential should have a leading jump at $z = 0$. If not, and in practical applications this is never the case due to the finite roughness of the air/film interface, the potential tends to 'drift away' from the $z = 0$ position. This translational invariance is not a serious problem, since the potential can easily be shifted back to the zero position, eventually by applying in a second run an appropriate phase change of the form $\exp(-\mathrm{i}kl)$ to the obtained complex reflection coefficient, if l is the required shift of the potential. The second condition to obtain a unique phase is that the (analytically extended) complex reflection coefficient should have no zero's in the upper half plane of the complex plane (UHP). Clinton derived several relations, using the Born approximation, for multilayers in terms of the SP's of the constituting layers that yield those systems with a reflection coefficient without zero's in the UHP, and that give thus a unique phase using equation (3) [15]. For real systems, however, a dynamical calculation has to be used, and then it appears that the thickness of the constituting layers and the roughness of the interfaces are intervening parameters that determine the number of zero's.

A program was developed, using the downhill simplex method, to determine the number and position of the zeros of the complex reflection coefficient in the UHP calculated by Parrat's recursive algorithm [1] for many different multilayer systems in the X-ray and neutron SP range. Then the SP was reconstructed using the procedures of Figure 1a to see the effects of the positions $(k_x, \mathrm{i}k_y)$ of the eventual zeros. The following trends were observed.

Firstly it appeared that the influence of the zero's introduced by the presence of interfacial roughness is most often negligible, if their values are not higher than about 1.0 nm. The zero's are normally located not too far from the real axis at values $k_x > 1.0$ nm^{-1} (and at $k_x < -1.0$ nm^{-1}), well beyond the critical edge k_c. In fact, the presence of moderate interface roughness quite often helps to improve the characteristics of the potential reconstruction of for example a thin film system, compared to that of the hypothetical system without interfacial roughness. The latter systems show quite often termination ripples around the sharp edges of the potential jumps due to finite wave transfer. This is naturally absent for multilayer systems with moderate interfacial roughness. Figure 4a shows several SP reconstructions as a function of the interfacial roughness for a thin film on a substrate system. Figure 4b shows the relative percentual error of the reconstructions of 4a (and others) as a function of the surface and the interfacial roughness. The reconstruction

gets worse if either the two roughness parameters are very different and/or one of the values is larger than 1.0 nm.

The second observation is that Clinton's relation for a single layer on a substrate is in first approximation correct, but need to be adapted for the influence of the film thickness. It was found that for a single film with constant SP V_f on a substrate with constant SP V_s there are no zero's in the UHP if $V_f > V_s$, regardless the thickness d of the film. This first relation is in accord with Clinton's findings. If however $(\Delta V_f/\Delta V_s) > 1$ where ΔV_f and ΔV_s are the heights of the two steps in V, respectively, and if $V_f < V_s$, there is a critical thickness d_{crit} beyond which phaseless inversion is no longer possible: $d > d_{crit} \approx \sqrt{1/V_s}(\Delta V_f/\Delta V_s)$. This phenomenological formula does not give exactly the critical thickness beyond which zero's appear in the UHP. For SP's in the X-ray range it is quite accurate, but for SP in the neutron range the formula tends to overestimate the real critical thickness. Tests with d-values below the phenomenological critical thickness, but above the real critical thickness, thus for systems with (usually) two zero's in the UHP, showed that phaseless inversion yields a completely satisfactory result. This is because the zeros are located very close to the real axis. The zeros thus have a very small imaginary part, rendering the phase correction important only for a few data points. The phenomenological formula thus accurately estimates the possible systems for phaseless inversion for either neutrons or X-rays. It is noted that the critical thickness is generally larger for neutrons than for X-rays for the same chemical system.

Clinton also derived a relation for multilayers: the largest jump in the scattering potential must be larger than the sum of the absolute values of all other jumps in order to be able to apply phaseless inverse scattering methods. Extensive simulations using the full dynamical theory have shown that this statement is remarkably correct, except for the important addition already found for the single-layer system. This means *in concreto* that the SP of a single layer within the multi-layer system must not be less than one half of the SP of all other layers. If it is larger than one half, but smaller than the SP of another layer, then its thickness must not exceed the critical thickness given by the phenomenological formula.

4 Experimental feasibility

It is shown now how PIS methods can be used, in conjunction with traditional fitting methods, to determine a non-trivial SP compatible with the experimental data. Three cases will be presented. The first one could be considered trivial, because the SP can be found with ease using traditional fitting methods. The two other examples are less evident to analyze using Parrat's recursive relations.

The first thin film was deposited by plasma enhanced chemical vapor deposition (PECVD) from diethoxydimethylsilane (DEDMS), resulting in an amorphous layer with $SiO_xC_yH_z$ composition [27]. The second film was a nominal 10 nm thick carbon layer obtained by cathodic sputtering, and the third one an approximately 14 nm thick C_4F_8 layer also obtained by PECVD from a 50%/50% C_4F_8/Ar plasma. All three thin films were deposited on clean (001) Si wafer surfaces.

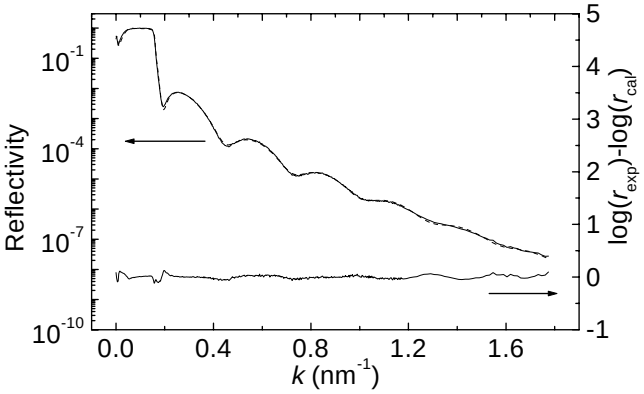

Fig. 5. Experimental X-ray reflectivity (full curve, left axis) from a DEDMS thin layer on a Si substrate and the reflectivity from the fitted single-layer model (dashed curve, left axis) and the corresponding difference curve (right axis). The parameters of the one-layer model are $\rho_{layer1} = 0.0176$ nm^{-2}, $\rho_{substrate} = 0.0248$ nm^{-2}, $d_{layer1} = 11.0$ nm, $\sigma_{air/layer1} = 0.64$ nm, $\sigma_{layer1/substrate} = 0.96$ nm.

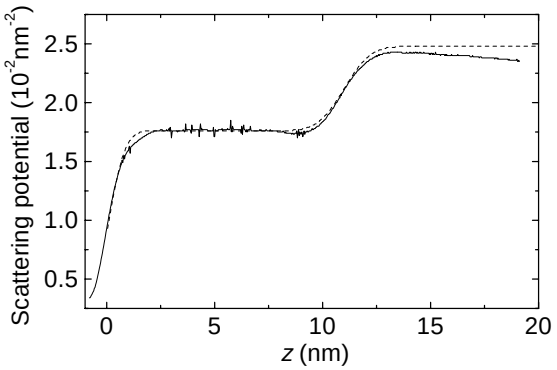

Fig. 6. SP of DEDMS film on a Si substrate determined by fitting using Parrat's scheme (dashed line), and by the PIS-method (full line).

X-ray reflectivity data were recorded using a commercial BRUKER D5000 diffractometer equipped with a reflectivity stage and a secondary graphite monochromator. The data were collected using Cu-$L_{3,2}$ X-rays ($\lambda = 0.154051$ nm and $\lambda = 0.15433$ nm, respectively) up to $k = 1.77$ nm^{-1}, $k = 1.22$ nm^{-1} and $k = 2.30$ nm^{-1}, for the DEDMS, carbon and the C_4F_8 film, respectively. Step sizes and counting times were variable, according to the intensity in a certain interval. The reflectivity intensity was recorded over 6 to 7 decades. Deconvolution of the data appeared not to be necessary, since the investigated films are rather thin.

Figure 5 presents the experimental data from the DEDMS-film along with the simulated data from a single-layer model fit using Parrat's recursive relations [1]. It is

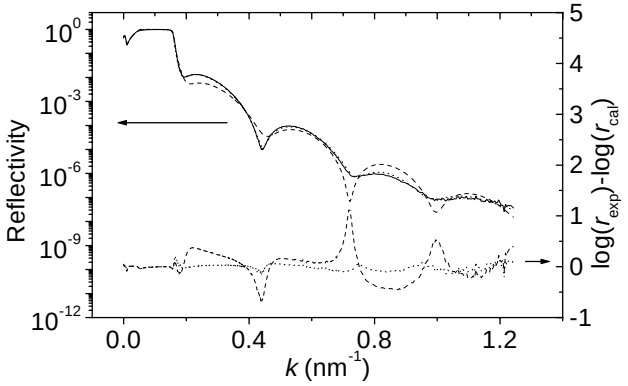

Fig. 7. Experimental X-ray reflectivity curve (full line, left axis) of a thin carbon film on a Si substrate and the difference curves (right axis) of the one-layer (dashed) and the two-layer (dotted) fit. The parameters of the one-layer model are $\rho_{\mathrm{layer1}} = 0.0202$ nm^{-2}, $\rho_{\mathrm{substrate}} = 0.0248$ nm^{-2}, $d_{\mathrm{layer1}} = 11.2$ nm, $\sigma_{\mathrm{air/layer1}} = 1.37$ nm, $\sigma_{\mathrm{layer1/substrate}} = 0.76$ nm. The parameters of the two-layer model are $\rho_{\mathrm{layer1}} = 0.0229$ nm^{-2}, $\rho_{\mathrm{layer2}} = 0.0169$ nm^{-2} $\rho_{\mathrm{substrate}} = 0.0248$ nm^{-2}, $d_{\mathrm{layer1}} = 7.7$ nm, $d_{\mathrm{layer2}} = 3.5$ nm, $\sigma_{\mathrm{air/layer1}} = 1.74$ nm, $\sigma_{\mathrm{layer1/layer2}} = 1.20$ nm, $\sigma_{\mathrm{layer1/substrate}} = 0.88$ nm.

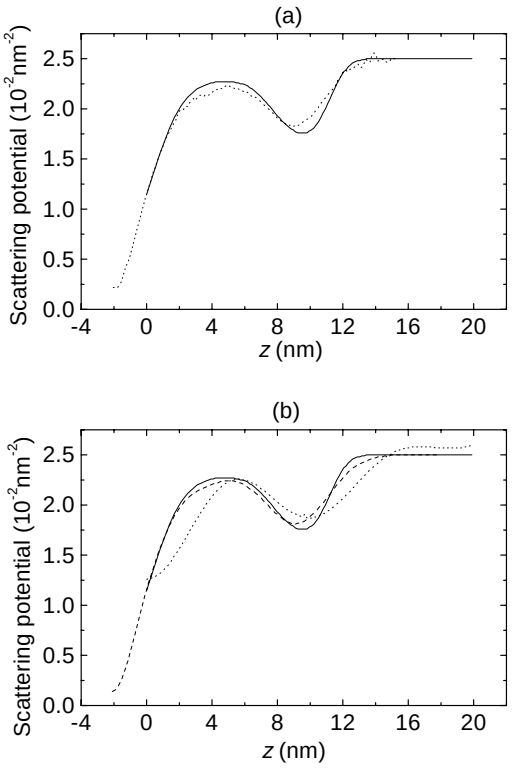

Fig. 8. (a) SP of carbon film on a Si substrate determined by fitting using Parrat's scheme (full line), and by the PIS-method (dotted line). (b) SP of carbon film determined by fitting using Parrat's scheme (full line), by the PIS-method using the complex reflection coefficient from Parrat's scheme at the experimental resolution (dashed line) and at a lower resolution $k = 0.400$ nm^{-1} (dotted line).

seen that the agreement between the curves is excellent, the reliability index being $R = 0.0078$. To prove that the *ab initio* determination of this trivial SP is also possible, the PIS calculations (Fig. 1a) using the experimental data were carried out. Figure 6 shows a good concordance between the PIS SP and the one-layer model from Parrat's fit. This trivial example demonstrates that PIS can be readily applied using experimental data collected with laboratory equipment. It appears that neither experimental noise, nor absorption for such a light-element system distorts the extracted PS. It is noted that the IS theory applied in this paper is intended for systems without absorption. This condition is normally fulfilled for neutron SP's, but X-ray SP's have normally an imaginary part. Finally it is verified experimentally that moderate interfacial roughness can be very well modeled.

The second example is not so trivial, in the sense that fitting using Parrat's recursive relations is not straightforward. The experimental reflectivity curve of the carbon film is shown in Figure 7 (full line). First a fit was tried using Parrat's recursive relations on the hypothesis that the layer is homogeneous (dashed line). The difference data $\log(r(k)_{\mathrm{exp}}) - \log(r(k)_{\mathrm{cal}})$ (lower part of Fig. 7, dashed line), on the same scale as the difference data in Figure 5 give the impression that the fit is only on the average correct. Taking into account the mean SP value resulting from the single-layer model fit, it could be anticipated that PIS methods could be useful to detect the deviations from the mean. Hence the SP was calculated following the PIS scheme of Figure 1a. Figure 8a shows the resulting SP as a dotted line. An density depleted region at the substrate/film interface results. A second fit using Parrat's scheme was tried with a two-layer model, that parametrized approximately the dotted curve of Figure 8a. The resulting difference data are given as the dotted line in the lower part part of Figure 7 at the same scale as the difference data of the one-layer model. The overall reliability indices are $R = 0.0659$ and $R = 0.0133$ for the one-layer model and two-layer model, respectively. The full curve in Figure 8a represents the two-layer model.

Since it is not known whether the real unknown complex reflection coefficient has zero's in the UHP and – more important – what their eventual influence is on the PIS determined SP, some further calculations were done. The UHP zero's of the complex reflection coefficient corresponding to the final two-layer model SP were calculated. There are indeed zero's in the UHP that find their origin in the rather large interfacial roughness. The first zero has a quite low real part $(\mathrm{Re}(k_0), \mathrm{Im}(k_0)) = (0.44, 0.011)$. The critical k_{c} vector of the substrate is $k_{\mathrm{c}} = 0.158$ nm^{-1}. If in turn this complex reflection coefficient is used for a PIS calculation, thus with neglecting the zero's, the dashed curve in Figure 8b results. The full curve represents again the two-layer SP that comes out of Parrat's fit; the dotted curve is the PIS SP calculated using the data at a much lower k-cutoff, *viz.*, at $k = 0.400$ nm^{-1}, thus just below the first zero in the UHP. It is noted that the dashed curve of Figure 8b is quite close to the dotted curve of Figure 8a

and that the general features of the curve are similar to that of the full curve. In other words: the PIS SP represents the zero-order approximation to the real SP.

By calculating the PIS SP an idea has been obtained how the SP could deviate from the single-layer model. Even the low-resolution data show up the reduced density layer at the substrate/film interface. It cannot be rigorously proved that the obtained SP is unique. That is only possible by an experimental determination of the phase. The full and dashed profile in Figure 8b give the same reflectivity amplitude, because the presence of UHP-zero's does not affect the amplitude. The final SP is anyhow better compatible with the experimental data than the original one-layer model, a result which should have been obtained with less ease by trial-and-error and/or least-squares fitting.

The third example, the nominally 14 nm thick C_4F_8 film, shows less deviations from the single layer model. Figure 9 (full curve) gives the experimental data along with the reflectivity resulting from the fit using a single-layer model (dashed curve). One could content oneself with this model, but one could also look for the reasons of the significant deviations between the two curves. It is noted that these deviations are truly significant when the experimental errors from counting statistics are taken into account. This error is maximum, about 4.5%, at the end of the experimental curve in Figure 9. Since the parameters of the single-layer model are in agreement with a SP that could be extracted by PIS, such a calculation was tried, resulting in the full curve of Figure 10. The dashed line in the same figure represents the single-layer model. It is seen that the PIS SP exhibits a slight, increasing density across the film. This density gradient is quite difficult to model with a limited number of layers in Parrat's recursive calculation method. Therefore Sanyal's model-independent fitting method was tried [2], taking the single-layer model (without roughness) as the unperturbed SP in the distorted wave born approximation. The thin layer was taken to be 16 nm and divided into 24 slices of equal thickness. The 24 points from the fit are very close to the (full) curve from the PIS calculation (Fig. 10). The reflectivity using this 24-layer model is in excellent agreement with the experimental data (Fig. 9, dotted curves).

Several comments can be made in comparing the *ab initio* PIS approach and Sanyal's model-independent fitting approach. Sanyal's method was found to be quite sensitive on the thickness of the thin layer to be modeled. Moreover, it is a pertubation method for which an unperturbed system has to be presumed that originates from a model-dependent fitting method. PIS is, on the other hand, really model-independent and uses no fitting whatsoever. Sanyal's method, however, does not suffer from the instability problems for larger potentials. In addition, it is not limited to potentials that fulfill the conditions of the phenomenological formula. It is seen that the PIS SP tends to level off for large z-values. This is a sign of the outset of instability. Both methods are in conclusion very sensitive to small deviations from an otherwise constant SP.

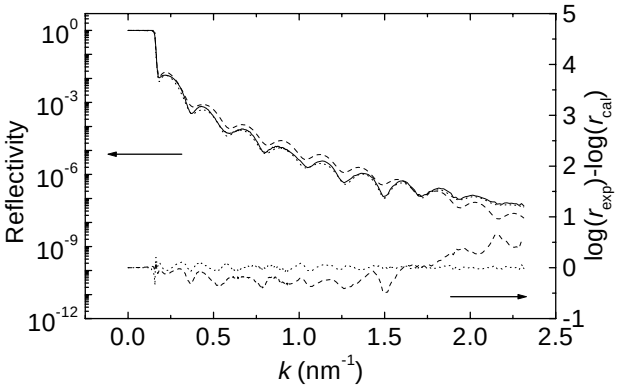

Fig. 9. Experimental reflectivity (full curve), together with their simulations calculated from the model resulting from Sanyal's fitting method (dotted) and from the one-layer model (dashed). The corresponding difference curves are shown in the lower part of the figure.

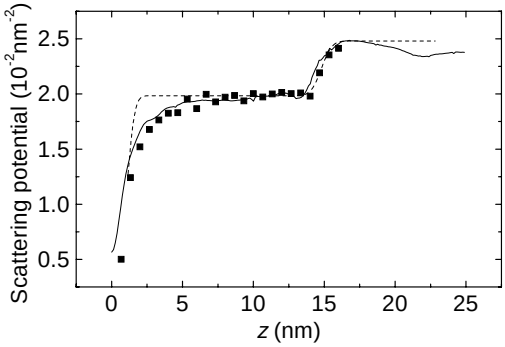

Fig. 10. SP of C_4F_8 film on a Si substrate determined by PIS (full line), by Sanyal's method (squares) and by classical fitting using Parrat's recursive relations (dashed line).

5 Concluding remarks

A new method to determine the scattering potential from specular reflectivity data using full dynamical theory, *viz.*, phaseless inverse scattering, has been tested on its experimental feasibility. The method has been previously described in literature, but has never been applied using experimental data. The phase extraction and the layer-stripping algorithms are stable against experimental noise, but fail for large potentials, even if the data are noise-free. It is shown for which systems PIS methods can extract a meaningful SP. When used with caution, PIS could provide valuable information complementary to traditional fitting methods, like those based on Parrat's recursive relations. PIS can detect deviations from multilayer-like models which are hard to find using the traditional fitting methods. PIS yields about the same information as Sanyal's method, but is intrinsically model-independent. However, the method gives, like Sanyal's and Parrat's method, rarely a unique SP, because of the lack of some fundamental *a priori* knowledge. Instead, more general IS methods have to be used to obtain a real unique SP, which

however require more laborious experiments that can quite often only be performed using a synchrotron or neutron source. Therefore, PIS could play an important role at a laboratory scale, when the possibility does not exist, for whatever reason, to perform more than one measurement or to change the system to be studied by the deposition of one or more reference layers.

S. Roualdes, D. Cot and H. Lecacheux (LMPM-Montpellier) are thanked for providing the DEDMS, carbon and C_4F_8 deposits, respectively.

References

1. L.G. Parrat, Phys. Rev. **95**, 359 (1954).
2. M.K. Sanyal, J.K. Basu, A. Datta, S. Banerjee, Europhys. Lett. **36**, 265 (1996).
3. J.S. Pedersen, I.W. Hamley, J. Appl. Cryst. **27**, 36 (1994).
4. N.F. Berk, C.F. Majkrzak, Phys. Rev. B **51**, 11296 (1995).
5. V.O. de Haan, A.A. van Well, S. Adenwalla, G.P. Felcher, Phys. Rev. B **52**, 10831 (1995).
6. C.F. Majkrzak, N.F. Berk, Phys. Rev. B **52**, 10827 (1995).
7. C.F. Majkrzak, N.F. Berk, J. Duna, S.K. Satija, A. Karim, J. Pedulla, R.D. Deslattes, Physica B (Utrecht) **241-243**, 1101 (1998).
8. A. Schreyer, C.F. Majkrzak, N.F. Berk, H. Grüll, C.C. Han, J. Chem. Phys. Sol. **60**, 1045 (1999).
9. M.K. Sanyal, S.K. Sinha, A. Gibaud, K.G. Huang, B.L. Carvalho, M. Rafailovich, J. Sokolov, X. Zhao, W. Zhao, Europhys. Lett. **21**, 691 (1993).
10. S. Banerjee, Y.J. Park, D.R. Lee, Y.H. Jeong, K.-B. Lee, S.B. Yoon, H.M. Choi, J.-C. Park, J.S. Roh, M.K. Sanyal, Appl. Surf. Sci. **136**, 41 (1998).
11. C.F. Majkrzak, N.F. Berk, Phys. Rev. B **58**, 15416 (1998).
12. T. Aktosun, P.E. Sacks, Inverse Pr. **14**, 211 (1998).
13. T. Aktosun, P.E. Sacks, Appl. Math. Rep. No. AM99-03, Iowa State University (1999).
14. M.V. Klibanov, P.E. Sacks, J. Math. Phys. **33**, 3813 (1992).
15. W.L. Clinton, Phys. Rev. B **48**, 1 (1993).
16. A. Gibaud, G. Vignaud, S.K. Sinha, Acta Cryst. A **49**, 642 (1993).
17. W. Bouwman, J.S. Pedersen, J. Appl. Cryst. **29**, 152 (1996).
18. A. Tikhonov, V. Arsénine, *Méthodes de résolution de problèmes mal posés* (MIR, Moscou, 1976).
19. W.H. Richardson, J. Opt. Soc. Am. **62**, 55 (1972).
20. L.B. Lucy, Astron. J. **79**, 745 (1974).
21. P.E. Sacks, J. Math. Phys. **38**, 3497 (1997).
22. T.M. Roberts, Physica B (Utrecht) **173**, 157 (1991).
23. P.E. Sacks, Wave Motion **18**, 21 (1993).
24. R. Lipperheide, G. Reiss, H. Leeb, H. Fiedeldey, S.A. Sofianos, Phys. Rev. B **51**, 11032 (1995).
25. H.J.S. Dorren, E.J. Muyzert, R.K. Snieder, Inverse Pr. **10**, 865 (1994).
26. H.J.S. Dorren (preprint, 1999).
27. S. Roualdes, A. van der Lee, R. Berjoan, J. Sanchez, J. Durand, AIChE J. **45**, 1566 (1999).